Carbohydrate Polymers 89 (2012) 623–631

Contents lists available at SciVerse ScienceDirect

Carbohydrate Polymers

journal homepage: www.elsevier.com/locate/carbpol

Water-soluble β-cyclodextrin grafted with chitosan and its inclusion complex as a mucoadhesive eugenol carrier

Warayuth Sajomsang[a], Onanong Nuchuchua[a], Pattarapond Gonil[a], Somsak Saesoo[a], Issara Sramala[a], Apinan Soottitantawat[b], Satit Puttipipatkhachorn[c], Uracha Rungsardthong Ruktanonchai[a,*]

[a] National Nanotechnology Center, National Science and Technology Development Agency, Thailand Science Park, Pathumthani, Thailand
[b] Department of Chemical Engineering, Faculty of Engineering, Chulalongkorn University, Bangkok, Thailand
[c] Department of Manufacturing Pharmacy, Faculty of Pharmacy, Mahidol University, Bangkok, Thailand

ARTICLE INFO

Article history:
Received 20 February 2012
Received in revised form 14 March 2012
Accepted 15 March 2012
Available online 28 March 2012

Keywords:
β-Cyclodextrin
Chitosan
Eugenol
Mucoadhesive
Surface plasmon resonance
Mucosal carrier

ABSTRACT

Inclusion complex between water-soluble βCD-grafted chitosan derivatives (QCD-*g*-CS) and eugenol (EG) was investigated as a new type of mucoadhesive drug carrier. The QCD-*g*-CSs were synthesized with various βCD moieties ranging from 5 to 23%. Spontaneous inclusion complex of these derivatives and EG were found and confirmed by FTIR and simulation study. Self-aggregated formations of QCD-*g*-CS were found, according to fluorescence and TEM studies, where the formations were preferable for QCD11*g*-CS and QCD5-*g*-CS. EG can be included in both βCD hydrophobic cavity and hydrophobic core of QCD-*g*-CS self-aggregates, resulting in varying entrapment efficiencies. Degree of QCD substitution on QCD-*g*-CS plays an important role on their physical properties, due to steric hindrance. The QCD11-*g*-CS showed excellent mucoadhesion, compared to the QCD5-*g*-CS and QCD23-*g*-CS. Moreover, the inclusion complex between QCD-*g*-CS and EG tend to express higher antimicrobial activities against *Candida albicans*, *Streptococcus oralis* and *Streptococcus mutans*, than the native QCD-*g*-CS.

1. Introduction

β-Cyclodextrins (βCD) are cyclic oligosaccharides having seven glucose units linked by α-(1,4) glucopyranose subunits, with a hydrophilic outer surface and a hydrophobic center cavity. The hollow lipophilic central cavity can accommodate a variety of hydrophobic guest molecules, due to hydrophobic interactions. It is well known that inclusion complex with CDs can significantly increase aqueous solubility of poorly soluble compound drugs, and thus improve stability of fragile compounds as well as controlled release (Szejtli, 2004). Chitosan (CS), a natural polysaccharide, obtained from deacetylation process, consists of β-(1,4)-2-amino-2-deoxy-D-glucopyranose units (GlcN) and a small amount of 2-acetamido-2-deoxy-D-glucopyranose or *N*-acetyl-D-glucosamine (GlcNAc) residues. It is used in various pharmaceutical works, due to its attractive non-toxic, biocompatibility, antimicrobial and mucoadhesive properties (Kumar, Muzzarelli, Muzzarelli, Sashiwa, & Domb, 2004; Muzzarelli et al., 1990). Due to advantages of both βCD and CS, their inclusion complexes with guest molecules, mucoahesive and antimicrobial properties, the βCD grafted with CS has been synthesized in many studies (Prabaharan & Gong, 2008; Prabaharan & Jayakumar, 2009; Prabaharan & Mano, 2005). This leads to various types of carrier that possess cumulative effects of inclusion, size specificity and transport properties of βCDs, as well as the controlled release ability of the polymeric matrix (Challa, Ahuja, Ali, & Khar, 2005).

Eugenol (EG) (4-allyl-2-methoxyphenol), a major phenolic component from clove oil (*Eugenia caryophyllata*, Myrtaceae), has demonstrated several biological activities including anti-inflammatory (Son, Kwon, Kim, Chang, & Kang, 1998), analgesic (Ohkubo & Shibata, 1997), anti-oxidation (Ou, Chou, Lin, Yang, & Sheu, 2006) and anti-bacterial against gram-positive and gram-negative microorganisms (Kalemba & Kunicka, 2003). However, light sensitivity and poor water solubility are major disadvantages of EG, as these limit practical uses. EG can be well-incorporated into αCD, βCD, and 2-hydroxypropyl-βCD (Zhan, Jiang, Wang, Li, & Dong, 2008; Yang & Song, 2005).

To achieve controlled drug release and better mucoadhesion of CD, water-soluble quaternized βCD-grafted CS (CD-*g*-CS) have been previously synthesized in our laboratory with the degree of *N*-substitution (DS) 5%, 11%, and 23% of βCD moieties (Gonil et al., 2011; Sajomsang et al., 2011). These derivatives were further quaternized by using glycidyl trimetylammonium chloride (GTMAC), (QCD-*g*-CS), in order to improve their water-solubility and mucoadhesive properties. In addition, we previously reported self-aggregates formation of these derivatives investigated using

* Corresponding author. Tel.: +662 564 7100x6552; fax: +662 564 6981.
E-mail address: uracha@nanotec.or.th (U.R. Ruktanonchai).

0144-8617/$ – see front matter © 2012 Elsevier Ltd. All rights reserved.
doi:10.1016/j.carbpol.2012.03.060

dynamic light scattering (DLS), atomic force microscopy (AFM), and transmission electron microscopy (TEM) (Sajomsang et al., 2011). This study was aimed to explore an ability of the synthesized QCD-*g*-CS derivatives to form inclusion complex with EG (QCD-*g*-CS-EG) and their mucoadhesive properties by using surface plasmon resonance (SPR). The antimicrobial activities of the QCD-*g*-CS-EG against *Candida albicans*, *Streptococcus oralis* and *Streptococcus mutans* were also compared to native QCD-*g*-CS.

2. Materials and methods

2.1. Materials

The following materials were acquired from the indicated sources without additional purification. Chitosan (CS) with an average molecular weight (M_w) of 22 kDa was acquired from Seafresh Chitosan (lab) Co., Ltd. (Thailand). The degree of deacetylation (DDA) of chitosan was determined to be 90% by ^{1}H NMR spectroscopy. β-Cyclodextrin (βCD) was from Wacker Chemical AG (Germany). p-Toluenesulfonyl chloride (TSCl) was from ACROS organic (Belgium). Glycidyltrimehylammonium chloride (GTMAC) and *N,N*-dimethylformamide (DMF) were from Fluka (Switzerland). Hydrochloric acid, acetic acid and sodium hydroxide were from Carlo Erba (Italy). Eugenol (EG) and mucin (type III) from porcine were from Sigma–Aldrich Co. (USA). Methanol, Na_2HPO_4, KH_2PO_4 and NaCl were from Fisher Scientific (UK). Sabourand's dextrose agar (SDA), Sabourand's dextrose broth (SDB), brain heart infusion agar (BHA), brain heart infusion broth (BHB) were from Becton (USA). MTT (3-(4,5-dimethyldiazol-2-yl)-2,5 diphenyl tetrazolium bromide, Dulbecco's modified Eagle's medium (DMEM) was from GIBCO Invitrogen (Grand Island, NY). Fetal bovine serum (FBS) was from Biochrom AG (Germany). L-Glutamine, penicilin G sodium, streptomicin sulfate, amphotericin B were from Invitrogen Corp. (USA). Dimethylsulfoxide (DMSO) was from Sigma–Aldrich, Inc, UK. Dialysis membranes with M_w cut-off of 12,000–14,000 g/mol from Cellu Sep T4 and Spectra/Por® MWCO 100–500 Da were purchased from Membrane Filtration Products, Inc. (Segiun, TX, USA) and Spectrum Laboratories Inc. (Rancho Dominguez, Canada), respectively. The water used for all experiments was deionized water from a MilliQ Plus (Millipore, Schwalbach, Germany). The microorganisms used in the inhibitory test were obtained from the Department of Medical Sciences, Ministry of Public Health, Thailand. Microorganisms used in the study were *Candida albicans* ATCC 10231 (*C. albicans*), *Streptococcus oralis* ATCC 35037 T (*S. oralis*) and *Streptococcus mutans* ATCC 25175 T (*S. mutans*).

2.2. Synthesis of β-cyclodextrin grafted with chitosan (CD-g-CS)

O-*p*-toluenesulfonyl-β-cyclodextrin (Ts-CD) was synthesized by a little modification of Brady, Lynam, O'Sullivan, Ahern and Darey's method (2000). The synthesis of CD-*g*-CS was carried out under acidic conditions and high temperature in the presence of DMF, which was previously reported by Gonil et al. (2011). Quaternized chitosan (QCS) and quaternized β-cyclodextrin grafted with chitosan (QCD-*g*-CS) were carried out by quaternization with GTMAC under acidic condition and high temperature which was previously reported (Gonil et al., 2011). The chemical structure of QCD-*g*-CS is shown in Fig. 1. The DSs were found to be 5 ± 2%, 11 ± 2%, and 23 ± 2% for QCD5-*g*-CS, QCD11-*g*-CS and QCD23-*g*-CS, respectively. It was found that the DS increased with decreasing DQ, was due to reduction of free primary amino groups of the CS backbone. The DQs were found to be 74 ± 1%, 65 ± 1%, and 60 ± 1% for QCD5-*g*-CS, QCD11-*g*-CS and QCD23-*g*-CS, respectively. These compounds are water-soluble due to a presence of quaternary ammonium moieties from GTMAC. The chemical characterization of QCD-*g*-CS has been previously reported (Gonil et al., 2011).

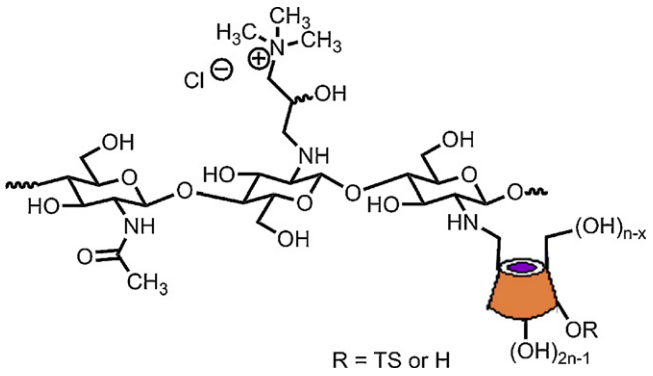

Fig. 1. Chemical structure of QCD-*g*-CS derivative.

2.3. Characterization of QCD-g-CS derivatives by FT-IR, ^{1}H NMR spectroscopy and molecular weight determination

FT-IR measurements were performed with a Nicolet 6700 spectrometer (Thermo Company, USA) with 32 scans and resolution of 4 cm^{-1} at ambient temperature (25 °C). ^{1}H NMR analysis was recorded with an ADVANCE AV 500 MHz spectrometer (Bruker, Switzerland). The measurement was performed at 300 K, using pulse accumulation of 64 scans and an LB parameter of 0.30 Hz. The weight average molecular weight (M_w) was determined by using the gel permeation chromatography (GPC). It consists of Waters 600E Series generic pump, injector, ultrahydrogel linear columns (M_w resolving range 1–20,000 kDa), guard column, pollulans as standard (M_w 5.9–788 kDa), and refractive index detector (RI). All samples were dissolved in acetate buffer pH 4. The mobile phases, 0.5MAcOHand 0.5MAcONa (acetate buffer pH 4), were used at a flow rate of 0.6 mL/min at 30 °C.

2.4. Computer modeling of inclusion complex between QCD-g-CS and EG

2.4.1. Thermodynamic properties of the inclusion complex in vacuum

The molecular dynamic simulations were performed using Material Studio version 4.3 (Accelrys, Boston, USA). A COMPASS force field was used throughout the study. The structures of βCD, QCD-*g*-CS with various DSs and DQs, and EG were constructed and subjected to geometry optimization. The optimized structures of EG were then subjected to an absorption locator module with various derivatives as absorption substrates. The models were constructed at fixed mole ratio of EG to βCD in QCD-*g*-CS at 1:1. Free energy of complex formation ($E_{complex}$) and the binding energy for the models, a summation of intra-molecular distortion ($E_{distortion}$) and inter-molecular interaction ($E_{non\text{-}bond}$) energy terms were expressed as:

$$E_{complex} = E_{distortion} + E_{non\text{-}bond} = (E_b + E_\theta + E_\phi) + (E_{vdW} + E_{Coulomb}) \quad (5)$$

where E_b is the bond stretching energy, E_θ is the valence angle bending energy, E_ϕ is the dihedral torsion energy, E_{vdW} is the Van der Waals interaction energy, and $E_{Coulomb}$ is the coulombic interaction energy.

2.4.2. Thermodynamic properties in water system

Models of QCD-*g*-CS and QCD-*g*-CS-EG inclusion complex were constructed as described above. The amorphous structures of

the host-guest inclusion complex were generated under periodic boundary conditions. The lengths of the cell were over 20.0 Å × 20.0 Å for the inclusion complex with the addition of 500 molecules of water to adjust in the system. The densities of βCD and EG in the systems were maintained in synthia units at 1.27 and 0.87 g/cm^3 at 298 K, respectively. Of ten configurations, only one system was chosen according to its lowest energy as given by molecular mechanics calculations as the initial configuration. To remove unfavorable interactions in the initial configuration, 5000 steps of energy minimization were employed using Smart algorithm.

Molecular dynamic simulation for 100 ps was carried out using normal pressure and temperature conditions with a time step of 1 femtoseconds (fs) in a range of 273–310 K. A cut-off distance of 9.0 Å and a buffer of 0.5 Å were adopted to minimize calculation of the non-bond interactions. Electrostatic charges of the model were calculated by the charge equilibration method. The duration of the equilibration dynamics was equal to100 picosecond (ps). Models of inclusion complex were then subjected to molecular dynamics for at least 1000 ps. Each of equilibrated EG: βCD in QCD-*g*-CS: water systems were then subjected to free energy calculation. The total free energy (ΔG) of each complex model in water-explicit system was calculated by the procedure proposed by Fermeglia's group (Fermeglia, Ferrone, Lodi, & Prici, 2003) as briefly described below. According to this method, ΔG_{bind} is calculated as follows:

$$\Delta G = \Delta G_{bind} + \Delta G^{C}_{sol} - \Delta G^{EG}_{sol} - \Delta G^{CD}_{sol} \quad (6)$$

where ΔG_{bind} is the complex formation energy ($E_{complex}$) between eugenol and βCD, ΔG^{C}_{sol}, ΔG^{EG}_{sol} and ΔG^{CD}_{sol} are the solvation free energy for the complex, eugenol and βCD, respectively.

All energetic analysis was performed only for a single molecular dynamic trajectory of the inclusion complex considered, with unbound βCD in QCD-*g*-CS and EG snapshots taken from the snapshots of that trajectory. The hydrogen calculation was performed by hydrogen build following this geometric parameter: the hydrogen-acceptor distance <3.0 Å and the donor-hydrogen-acceptor angle >90.0°.

2.5. Preparation of inclusion complex

The 0.2 g of QCD-*g*-CS was dissolved in 10 mL of deionized water. The EG was then added at the molar ratios of 1:1 (QCD-*g*-CS:EG). The mixtures were stirred at 25 °C at a speed of 250 rpm for 4 h. The inclusion complex was lyophilized using a freeze dryer (CRYODOS-80, Telstar, Spain). The obtained powders were stored in gas-tight bottles at −20 °C until further analysis.

2.6. Fourier transform infrared (FTIR) spectroscopy

Formation of the inclusion complex was verified by infrared spectroscopy (FTIR, Perkin–Elmer, USA) in the frequency range between 4000 and 400 cm^{-1}. The infrared spectra of EG and QCD11-*g*-CS (QCD11-*g*-CS-EG) inclusion complex at 1:1 mole ratio were recorded and analyzed in comparison with those of EG, QCD11-*g*-CS and physical mix between EG and QCD11-*g*-CS.

2.7. Dynamic light scattering (DLS) measurement

The self-assemblies in aqueous solutions were investigated with photon correlation spectroscopy (PCS) (NanoZS4700 nanoseries, Malvern Instruments, UK). The 2% (w/v) QCD-*g*-CS samples were dissolved into deionized water. The refractive index of samples and water was set at 1.33. Droplet size was obtained as the average of three measurements at 25 °C.

2.8. Morphology analysis

The self-assemblies were observed by transmission electron microscopy (TEM) using high resolution electron microscope (JEM-2010, Japan) operating at an acceleration voltage of 300 kV. 2%w/v QCD-*g*-CS was dissolved in deionized water. Samples were prepared at 25 °C by dropping on carbon-coated copper grids, and the extra solution was blotted with filter paper. After the water was evaporated at room temperature, the samples were stained by phospho-tungstic acid (1%, w/v) for 1 min and observed.

2.9. Critical aggregation concentration (CAC) measurement

Using pyrene as a fluorophore, steady-state fluorescence spectra were measured on fluorescence spectrophotometer (Perkin Elmer, precisely LS55) with a 5-nm width slit for both excitation and emission. The 10 μL of pyrene solution (2 mg/100 mL) was added into QCD-*g*-CS solution in the concentration range of 0.04–0.2 mg/mL. For self-assembly formation, the mixtures were further sonicated before incubating at 50 °C for 2 h. All tests were carried out at 25 °C. The sensitive fluorescent intensity was marked at 373 nm (I_{373}) and 383 nm (I_{383}). I_{373}/I_{383} was then calculated and plotted against log of QCD-*g*-CS concentrations.

2.10. Determination of EG entrapment efficiency (EE)

The amount of EG included in inclusion complex was determined by an extraction. The inclusion complex was mixed with methanol. The mixture was vigorously shaken at 60 °C at a speed of 250 rpm for 8 h. The supernatants were separated by centrifugation (MR231, Thermo Scientific, USA) under 7500 rpm, 30 °C for 30 min, and then EG content was measured by UV spectrophotometer (Lamolecular Dynamica 650, Perkin Elmer, USA) at the wavelength of 281 nm. All measurements were performed in triplicate and averaged. The percentage of entrapment efficiency (%EE) can be calculated as follow:

$$\%EE = \frac{\text{amountof extracted eugenol(mg)in methanol} \times 100}{\text{amount of added eugenol(mg)}} \quad (1)$$

2.11. Mucoadhesion by surface plasmon resonance (SPR)

The mucoadhesive properties of QCD-*g*-CS and their inclusion complex with EG were determined by SPR according to the BIACORE method (Thongborisute & Takeuchi, 2008) and the method has been modified (Petchsangsai et al., 2011). CMD500 (carboxymethyldextran hydrogel) sensor chip surface was pre-activated with a mixture of 100 mM N-hydroxysuccinimide (NHS) and 400 mM 1-ethyl-3-(3-dimethylaminopropyl) carbodiimide hydrochloride (EDC). Mucin particle suspension at a concentration of 0.1% (w/v) was prepared in 10 mM acetate buffer (pH 4.5). All immobilization were carried out at a flow rate of 50 μL/min. First, 22 kDa chitosan was injected at a concentration of 0.1% (w/v). The remaining reactive esters were transformed into inactive amides by injection of 1 M ethanolamine HCl, pH 8.5, at a flow rate of 50 μL/min. After collecting the equilibrium baseline data, mucin particle suspension was injected followed by 0.5% (w/v) of samples. The refractive index unit (RIU) for each sample was then recorded on the home-built SPR imaging system equipped with a 7-channel flow cell. Details of the SPR imaging apparatus, similar to the system previously reported (Shumaker-Parry, Aebersold, & Campbell, 2004). Polyacrylic acid (~140 kDa) was used as positive control in this study. The percentage of RIU (%RIU) change was analyzed according to the equations below after the injections of samples and NaCl, respectively.

$$\%\,\text{RIU change} = \frac{\text{RIU baseline of sample} - \text{RIU baseline of mucin}}{\text{RIU baseline of mucin} - \text{RIU baseline of immobilized chitosan}} \times 100 \quad (2)$$

$$\%\,\text{RIU change (with NaCl)} = \frac{\text{RIU baseline of NaCl} - \text{RIU baseline of mucin}}{\text{RIU baseline of mucin} - \text{RIU baseline of immobilized chitosan}} \times 100 \quad (3)$$

2.12. Viscosity analysis

Viscosities were measured using rotational (controlled stress) rheometer (Model Gemini 200HR Nano, Malvern Instruments, UK) with a 55 mm diameter cone-plate at 25 °C. 0.6 mL of 1% w/v sample was adequately filled in a 200 μm space between a cone-plate and basement. The viscosity was recorded at a shear rate of 1000 s^{-1}.

2.13. Determination of antimicrobial activity

S. oralis and *S. mutans* and *C. albicans* at the initial concentration of 10^7 CFU/mL was mixed with either QCD-*g*-CSs or their inclusion complex with EG, where the broth was used as a negative control. After 24 h incubation at 37 °C, appropriate dilutions of each microbe were spread on agar medium using a spiral plate (Autoplate 4000; LABEQUIP Ltd., Ontario, Canada). The plates were then incubated at 37 °C for 24 h and bacterial count was made based on total number of viable cells in units of CFU/mL. Each measurement was performed in triplication.

$$\%\,\text{Bacterial reduction} = \frac{(\log A - \log B) \times 100}{\log A} \quad (4)$$

where % bacterial reduction is percentage of bacteria reduction, log *A* is log number of bacteria colonies from broth as a negative control, and log *B* is log number of bacteria colonies from the QCD-*g*-CSs or their inclusion complex with EG.

3. Results and discussions

3.1. Synthesis and characterization of QCD-g-CS

The synthesis of water-soluble CD-*g*-CSs was carried out by quaternizing the CD-*g*-CS with GTMAC under acidic condition. The chemical structure of QCD-*g*-CS is shown in Fig. 1. The degree of N-substitution of βCD in QCD-*g*-CS (DS) determined by ^{1}H NMR method were found to be 5 ± 2%, 11 ± 2%, and 23 ± 2% for QCD5-*g*-CS, QCD11-*g*-CS and QCD23-*g*-CS, respectively. FT-IR spectra of QCD-*g*-CS showed the characteristic peak at wavenumber of 1473 cm^{-1} due to C—H stretching of the methyl substituent of quaternary ammonium groups. The characteristic absorption band of the βCD and CS were found in QCD-*g*-CS such as at wavenumbers of 1593 and 1121–1005 cm^{-1} corresponded to N—H deformation of amino groups and the symmetric stretching of the C—O—C and involved skeletal vibration of the C—O stretching, respectively. The ^{1}H NMR spectrum of the QCD-*g*-CS showed the doublet proton signals at δ 7.4–7.0 ppm, corresponding to the aromatic protons. The proton signal at 5.3 ppm was assigned to the H1′ proton of the GlcN whereas the proton signal at δ 4.9 ppm was assigned to the H1 proton of βCD. Moreover, the multiplet proton signals at 5.0–3.0 ppm were corresponded to the protons of βCD, and the proton signals at 3.1 and 2.7 ppm were assigned to the quaternary ammonium proton and methylene proton, respectively. The recoveries of QCD-*g*-CS were found to be 66, 79 and 71% for QCD5-*g*-CS, QCD11-*g*-CS and QCD23-*g*-CS, respectively.

3.2. Computer modeling on complex formation between EG and QCD-g-CS

Table 1 shows binding energy, solvation energy and total free energy of interaction between EG and βCD, CS and QCD-*g*-CS at 1:1 mole ratio of inclusion complex. According to negative values of these energies, EG could favorably interact with either (CD or CS backbone. Total free energy of EG against βCD and backbone CS were found to be −711.26 kcal mol^{-1} and −237.16 kcal mol^{-1}, respectively. It was clearly indicated that inclusion complex between EG and βCD was significantly more favorable than the interaction between EG and CS. Notably, negative energetic term results not only come from EG binding interactions with βCD cavity or CS backbone, but also from solubility of βCD and CS chain as well as its final complex. The calculated solvation energy suggested that EG forms stable inclusion complex with βCD more than CS, which could result from better water-solubility of βCD than CS.

Models of EG and QCD-*g*-CS derivatives in aqueous system subjected to molecular dynamic simulations are presented in Fig. 2. The energetic calculations were obtained from a snapshot of each molecular dynamic trajectories between EG and QCD-*g*-CS derivatives. Total free energy changes of QCD5-*g*-CS, QCD11-*g*-CS and QCD23-*g*-CS with EG are negative, suggesting that they can spontaneously form inclusion complex with EG. According to total free energy, the stability of inclusion complex can be ranked as QCD11-*g*-CS-EG (−120.70 kcal mol^{-1}) > QCD5-*g*-CS-EG (−59.39 kcal mol^{-1}) > QCD23-*g*-CS-EG (−2.92 kcal mol^{-1}). Therefore, % grafting of (CD into the CS backbone plays a major role on free energy of binding and the stability of inclusion complex with EG. Negative energetic terms result not only from non-bond interactions between EG and the grafted βCD cavities, but also from solubility of QCD-*g*-CS and its final inclusion complex. The remarkable energetic terms described the required energy for desolvation of QCD-*g*-CS and solvation energy of the complexes.

Models of equilibrated QCD-*g*-CS-EG inclusion complex of QCD5-*g*-CS-EG, QCD11-*g*-CS-EG and QCD23-*g*-CS-EG were stable throughout the simulated period. However, alignments of EG molecule in the βCD cavity were different (Fig. 2). In most stable complex forms, hydrophobic portion of EG molecules are enclosed within βCD. The hydrophilic portion of the EG molecules are exposed to aqueous environment as water molecules are still associated with the hydrophilic portion of EG. QCD-*g*-CS and EG inclusion complex could occur by an absorption of EG on the external surface of QCD-*g*-CS-EG. Therefore energetic favorable complexes were observed throughout molecular dynamic of surface absorbed model of QCD5-*g*-CS, QCD11-*g*-CS and QCD23-*g*-CS due to high negative values of total free energy. However, surface absorbed model of QCD5-*g*-CS was not stable (data not shown) because of low content of (CD moiety into QCS backbone.

Table 1
Comparison of the binding energy and thermodynamic characteristics of βCD, CS and QCD-*g*-CS with EG in aqueous system.

Energy (kcal mol^{-1})	βCD	CS	QCD5-*g*-CS	QCD11-*g*-CS	QCD23-*g*-CS
Binding energy	−16.41	−46.63	−22.69	−20.23	−22.31
Solvation energy	−695.21	−162.06	−36.70	−100.47	19.40
($G^{complex}$	−9022.67	−8273.90	−1069.91	−1522.21	−310.43
($G^{derivatives}$	−8273.90	−6446.31	−997.77	−1386.31	−294.39
($G^{eugenol}$	−53.54	−53.54	−35.44	−35.44	−35.44
Total free energy	−711.26	−237.16	−59.39	−120.70	−2.92

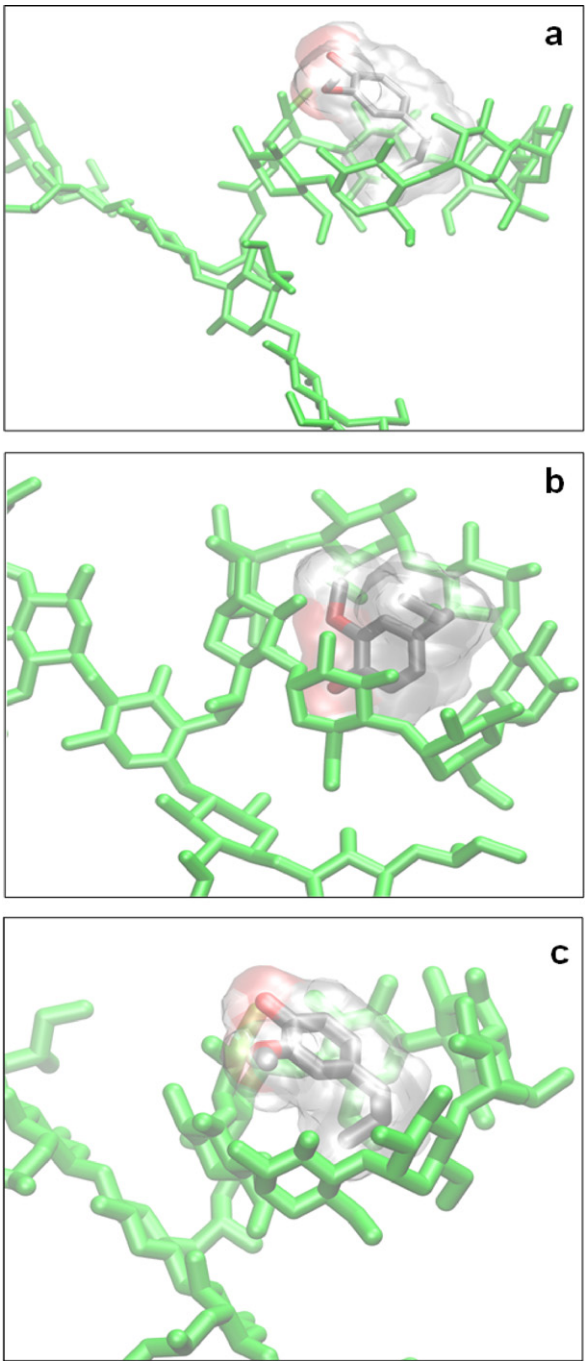

Fig. 2. Host–guest C–H:O interactions between EG (grey spheres) and QCD5-*g*-CS-EG (a), QCD11-*g*-CS-EG (b) and QCD23-*g*-CS-EG (c) (green lines) at 1:1 mole ratio. (For interpretation of the references to color in this figure legend, the reader is referred to the web version of the article.)

3.3. Complex formation between EG and QCD-g-CS

FTIR spectra of EG, native QCD11-*g*-CS, QCD11-*g*-CS-EG inclusion complex at 1:1 mole ratio and its physical mix are shown in Fig. 3. The QCD11-*g*-CS demonstrated dominant peaks at wavenumbers 3417 cm^{-1}, 1030 cm^{-1}, and 1473 cm^{-1} due to O—H stretching, C—O stretching of CS backbone, and C—H stretching of the methyl substituent of quaternary ammonium groups, respectively. The EG showed its signature peaks at wavenumbers 1640, 1610, 1510, and 558–998 cm^{-1} which are corresponding to C=C stretching and C—H bending of the alkene/aromatic groups in EG structure. For physical mix, three peaks at wavenumbers 1640,

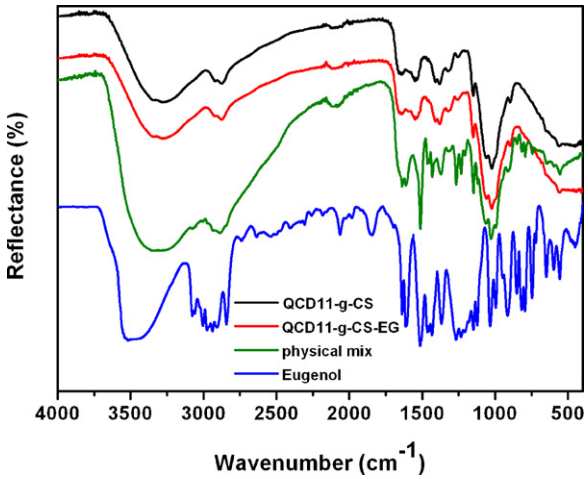

Fig. 3. FTIR spectra of QCD11-*g*-CS, QCD11-*g*-CS-EG inclusion complex at 1:1 mole ratio, physical mix (QCD11-*g*-CS and EG at 1:1 mole ratio) and eugenol.

1610 and 1510 cm^{-1} were found, suggesting C=C stretching of the aromatic moiety. The spectra of these peaks were similar to those existed in EG, confirming a presence of EG in the physical mix. On the other hand, no characteristic peaks of EG were observed in QCD11-*g*-CS-EG inclusion complex. This could be due to inclusion complex formation between EG and QCD11-*g*-CS. Another possible mechanism is that the EG can be encapsulated in hydrophobic core of QCD11-*g*-CS. However, it should be noted that no peak of new functional group was found, suggesting non-bond host–guest interaction.

3.4. Self-aggregated formation of QCD-g-CS

Apart from host-guest interactions between EG and hydrophobic cavity of QCD-*g*-CS, self-aggregated formation of QCD-*g*-CS is also expected to occur in aqueous system. Nanoaggregates of native CDs in water have been reported, which mainly depend on the CDs considerably (Coleman, Nicolis, Keller, & Dalbiez, 1992; He, Fu, Shen, & Gao, 2008). Moreover, modified CDs and inclusion complex of CDs are able to form larger aggregates in aqueous solutions (Auzely-Velty, Djedaini-Pilard, Desert, Perly, & Zemb, 2000; Zhang, Feng, Cuddihy, Kotov, & Ma, 2010). We previously reported self-aggregated formation of QCD-*g*-CS by using DLS, AFM and TEM (Sajomsang et al., 2011). We found that the sizes of self-aggregates increased with an increasing in DS into the CS backbone, indicating that more CDs substitution leading to larger aggregates in water.

In this study, the self-aggregation of inclusion complex was investigated by fluorescence study. Pyrene was chosen as the fluorescence probe because its condensed aromatic structure is sensitive to polarity, and can produce distinctive fluorescence under conditions of sufficient high concentration and mobility. Fig. 4a shows the fluorescence emission spectra of pyrene at various concentrations of the QCD5-*g*-CS. No significant change in the total fluorescence intensity was found at low concentration range, indicating that the QCD-*g*-CS did not form self-aggregate at diluted QCD-*g*-CS concentration. An increase in the excimer intensity (420–500 nm) was observed with an increasing in the QCD-*g*-CS concentration while the excimer formation was not observed in the case of βCD solutions. In comparison to the βCD, the broadening of the emission bands of pyrene was observed in the presence of all QCD-*g*-CS at the concentration of 2 mg/mL (Fig. 4b). This result indicates that QCD-*g*-CS start to form hydrophobic domains in aqueous media resulting from intermolecular hydrophobic interactions at a certain concentration, which was defined as the critical aggregation concentration (CAC), meaning the threshold concentration of

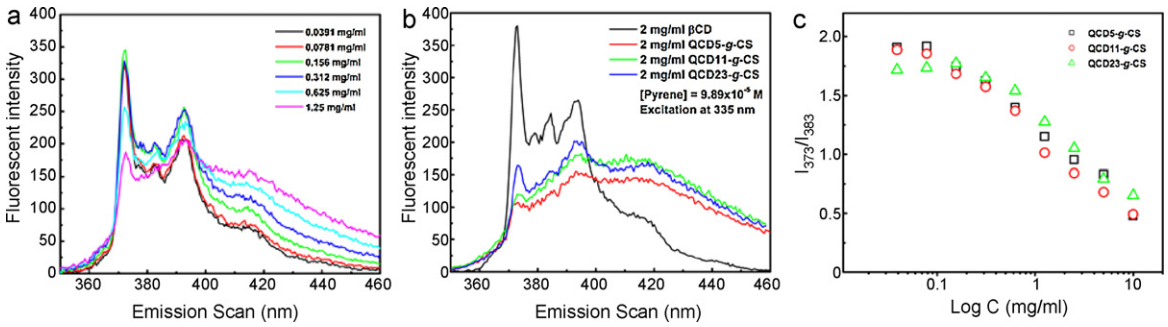

Fig. 4. Fluorescence emission spectra of pyrene at various concentrations of the QCD5-*g*-CS (a), QCD-*g*-CSs at the concentration of 2 mg/mL (b) and plots of I_{373}/I_{383} as a function of the concentration of all QCD-*g*-CSs.

self-aggregation of polymeric amphiphiles or QCD-*g*-CS. The CAC can be determined by observing the change in the intensity ratio of the pyrene in the presence of QCD-*g*-CS (Tan & Liu, 2009).

Fig. 4c shows the intensity ratio (I_{373}/I_{383}) of the pyrene excitation spectra *versus* the logarithm of the QCD-*g*-CS concentration. At low concentrations of QCD-*g*-CS, the *I*373/*I*383 values are closed to the value 2.0, which remains nearly unchanged. The intensity ratios begin to decrease with increasing concentration of QCD-*g*-CS. The CAC is determined by the interception of two straight lines. The CAC values of QCD5-*g*-CS, QCD11-*g*-CS, QCD23-*g*-CS were found at 0.156, 0.156 and 0.312 mg/mL, respectively. These CAC results confirm a formation of self-aggregates of QCD-*g*-CS at varying extent depending on DS. It is likely that EG was included not only in βCD hydrophobic cavity of QCD-*g*-CS, but also in hydrophobic core of QCD-*g*-CS self-aggregates. Schematic structure of self-aggregates between QCD-*g*-CSs and EG was proposed in this study as shown in Fig. 5.

The QCD-*g*-CS entrapped with EG was further investigated using dynamic light scattering (DLS) and transmission electron microscopy (TEM). Fig. 5 shows TEM image of the QCD5-*g*-CS assembly where spherical particles were observed with a diameter in a range of 300–900 nm. According to TEM images, the mean size of the assemblies formulated with QCD5-*g*-CS-EG, QCD11-*g*-CS-EG, QCD23-*g*-CS-EG were 317 ± 48, 893 ± 84 and 617 ± 71 nm, respectively whereas from DLS were 1024 ± 56, 1122 ± 98 and 657 ± 45 nm, respectively. Moreover, there is a large discrepancy in the obtained size from TEM and DLS which could be due to the method of preparation. For the TEM measurement, material dehydration during sample preparation may occur, whereas for the DLS measurement the particles were suspended in an aqueous medium or in a swelling state. Therefore, smaller particle sizes from TEM measurements as compared to DLS have been obtained and are in agreement with previous report (Anantachaisilp et al., 2010).

3.5. Determination of EG entrapment efficiency (%EE)

The amount of EG entrapment both in βCD cavity and hydrophobic core of QCD-*g*-CS were investigated from inclusion complex at 1:1 mole ratio between QCD-*g*-CS and EG. The EG entrapment efficiency (%EE) of EG from QCD5-*g*-CS, QCD11-*g*-CS and QCD23-*g*-CS was found to be 63.8 ± 1.3%, 77.5 ± 7.4% and 59.3 ± 2.4%, respectively. The results revealed that the DS affected on %EE. At the same mole ratio of 1:1, it was expected that a presence of higher DS of QCD23-*g*-CS would result in higher βCD, leading to higher %EE as compared to QCD11*g*-CS or QCD5-*g*-CS. However this does not seem to be the case in which the lowest %EE was obtained from QCD23-*g*-CS. Therefore, these indicate that EG entrapment in hydrophobic core of QCD-*g*-CS self-aggregates plays a role on % EE values. Notably, % EE results corresponded well with CAC values from pyrene fluorescence study (Fig. 4) where CAC values of QCD11*g*-CS and QCD5-*g*-CS were the same (0.156 mg/mL) and much lower than that of QCD23-*g*-CS (0.312 mg/mL), indicating that self-aggregated formation were more preferable for QCD11*g*-CS and QCD5-*g*-CS. It should be noted that the highest amount of EG can be entrapped within both βCD cavity and hydrophobic core of QCD11-*g*-CS than other QCD-*g*-CSs. This result also correlated well with simulation study where total free energy of QCD11-*g*-CS was the most preferable and QCD23-*g*-CS was the least. It is possible that the QCD-*g*-CS may itself have an impaired ability to form inclusion complex with EG as a result of changes in its conformational structure or obstruction of its cavity, upon the optimization of DS in QCD-*g*-CSs (Bibby, Davies, & Tucker, 1999). The decrease in complexing ability of QCD23*g*-CS and EG could be attributed to steric hindrance of βCD itself or remained tosylate group into the QCD-*g*-CS backbone. This was consistent with Pitha, Harman, and Michel (1986) and Yoshida, Arima, Uekama, and Pitha (1988), who found that the complex ability of βCD derivatives toward various guest molecules decreased with increasing DS. In this respect, the role of DS level should be considered. Our results confirm that the DS plays an important role on complex formation between EG and QCD-*g*-CS.

3.6. Mucoadhesion by surface plasmon resonance (SPR) and viscosity study

According to the principle of the BIACORE method described by Takeuchi, Thongborisute, Matsui, Yamamoto, & Kawashima, (2005), if the binding between mucin and the polymers occurs, the response on a prepared sensor surface should increase as the sample passes over. Moreover, if equilibrium is reached, a constant signal is seen. Therefore, the strength of binding can be determined by changing the percentage of refractive index unit (%RIU) response (Thongborisute & Takeuchi, 2008). Mucoadhesive properties of QCD-*g*-CS and quarternized CS (QCS) were investigated (Table 2). In this study, polyacrylic acid (PAA) was used as a positive control. After injection of mucin, the %RIU response increased due to immobilization of mucin on sensor chip surface. An increase in %RIU response led to the change of refractive index on the sensor chip surface when a binding between injected molecules (mucin) and immobilized molecules (CS) occurred. When either QCD-*g*-CSs or QCS was exposed on the mucin-immobilized sensor chip surface, the %RIU response was increased. This can be explained by the ability of the CS derivatives to hold mucin particles on the sensor chip surface, leading to aggregation of the mucin from the sensor surface. Notably, this is due to electrostatic interactions between positively charged of quaternary ammonium groups of CS derivatives and negatively charged groups of sialic acid and sulfated sugars in mucin (Svensson, Thuresson, & Arnebrant, 2008). The values of an increase in %RIU response of QCD5-*g*-CS, QCD11-*g*-CS, and QCD23-*g*-CS were 43.58, 56.72, and 11.79, respectively while the

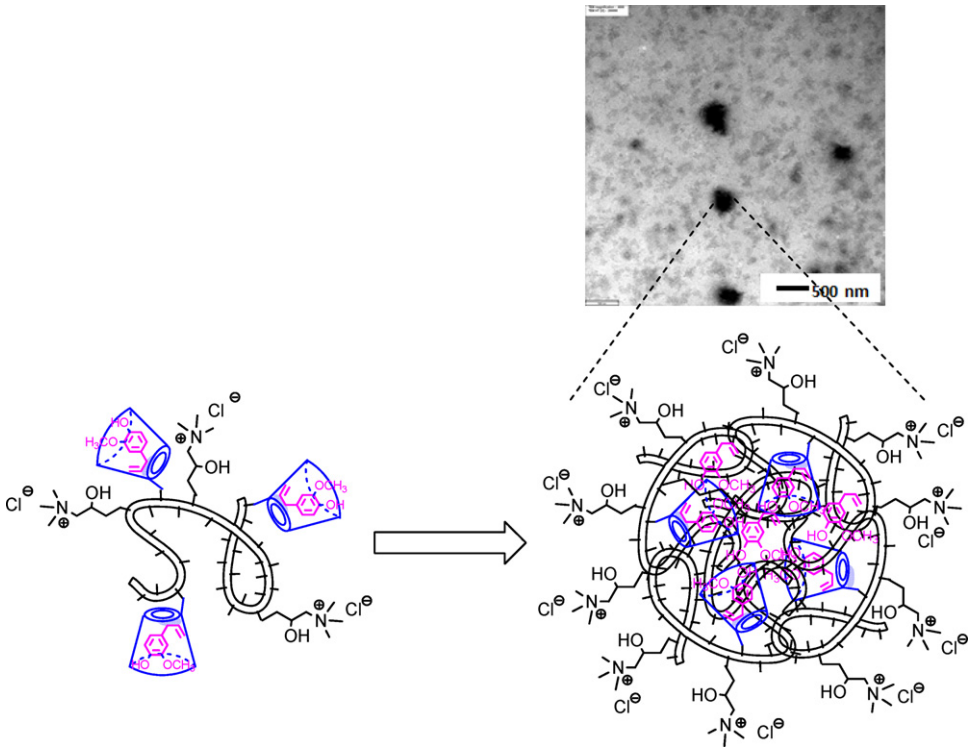

Fig. 5. Schematic structure of EG with self-aggregates of quaternized cyclodextrin grafted with chitosan (QCD-*g*-CSs) and TEM image of inclusion complex between EG and QCD5-*g*-CS.

%RIU change of PAA was only 27.65, which was less than those of QCD-*g*-CS. A greater mucoadhesion was found from QCD11-*g*-CS than those of QCD5-*g*-CS and QCD23-*g*-CS. However, the highest %RIU change (75.57) was obtained from QCS, which was another positive control in this study. In comparison to native QCD-*g*-CS, the %RIU responses of QCD-*g*-CS entrapped with EG were not significantly different. A viscosity measurement of these QCD-*g*-CS derivatives was performed at 1000 s^{-1} to support the SPR results since a viscosity analysis has been employed as one factor to determine mucoadhesive property of new materials based on the ability of the material to be retained on mucosal surfaces for extended periods (Smart, 2005). The process, in which material dispersions spread and are retained on mucosa depend principally on the surface energy of the mucosal surfaces and the material, along with the rheology of the material. The obtained viscosity values can be ranked as QCS (14.83 cps) > QCD11-*g*-CS (3.09 cps) > QCD5-*g*-CS (2.54 cps) > QCD23-*g*-CS (1.93 cps) > PAA (0.89 cps) and these values correlated well with the SPR results. However, there are many factors that affected viscosity such as molecular weight, molecular size, molecular shape, intermolecular force, temperature, and concentration. In comparison to QCS, introduction of βCD moieties into the QCD-*g*-CS backbone led to reduction of molecular weight and viscosity (Table 2). The QCD11-*g*-CS showed the highest molecular weight compared to other QCD5-*g*-CS and QCD23-*g*-CS. Moreover, high DS of QCD23-*g*-CS may reduce of intermolecular hydrogen bonding during QCD-*g*-CS backbone, leading to reduction of viscosity. Therefore, the DS affects most on mucoadhesive response of the derivative where an optimal DS at 11% demonstrate the highest %RIU as compared to others.

An injection of 3 M sodium chloride was performed at the last phase in order to define interaction between mucin particle and these CS derivatives. Our hypothesis is that an increase in ionic strength of sodium chloride results in the detachment of mucin and QCD-*g*-CS. It was found that a large decrease in %RIU response was found in case of QCD-*g*-CS, whereas a small decrease in %RIU response was observed with QCS. In addition, only little effect on %RIU response of PAA was obtained (Table 2). These results suggested that electrostatic interaction play a major role in governing the adhesion between mucin and the QCD-*g*-CS derivatives. Another mechanism such as hydrogen bonding is possible to govern the interaction. In our case, the mucoadhesive activity of these derivatives were from not only electrostatic interaction between positively charges of QCD-*g*-CSs and negatively charges of mucin, but also the viscosity of native QCD-*g*-CS and their complexes (Rossi, Ferrari, Bonferoni, & Caramella, 2001).

3.7. Antimicrobial activity

Antimicrobial activities of EG and their inclusion complex with QCD-*g*-CSs were investigated against three microorganism

Table 2
Mucoadhesive properties, viscosity and weight average molecular weight (M_w) characteristics of QCD-*g*-CS with and without EG.

Concentration (0.5%, w/v)	% RIU response			Viscosity at shear rate of 1000 s^{-1} (cps)	M_w (kDa)
	Without EG	With EG	NaCl injection		
PAA	27.65 ± 0.72	–	5.58 ± 1.40	0.89	140.0
QCS	75.57 ± 9.56	–	−8.74 ± 12.33	14.83	97.45
QCD5-*g*-CS	43.58 ± 0.07	45.24 ± 0.10	−79.03 ± 1.08	2.54	75.67
QCD11-*g*-CS	56.72 ± 0.19	52.44 ± 0.44	−79.89 ± 1.09	3.09	81.24
QCD23-*g*-CS	11.79 ± 0.42	6.89 ± 0.35	−56.52 ± 0.41	1.93	74.56

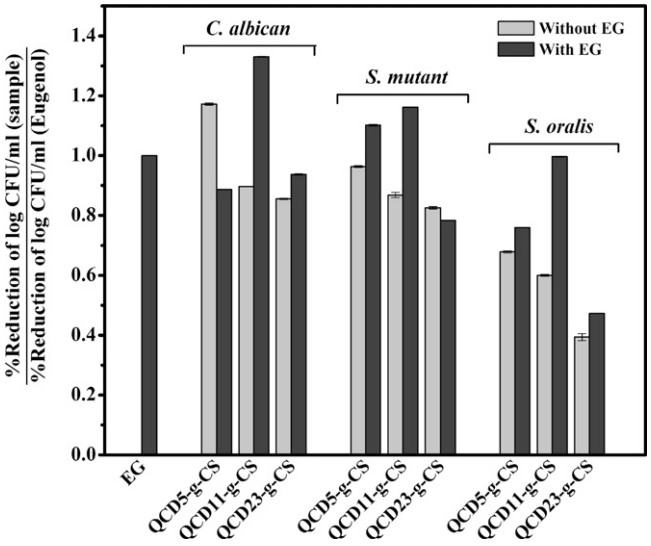

Fig. 6. Antimicrobial activity of βCD and QCD-*g*-CS derivatives (QCD5-*g*-CS, QCD11-*g*-CS and QCD23-*g*-CS) on *C. albican*, *S. mutant* and *S. oralis* after 24 h of incubation at 37 °C.

(*C. albican*, *S. mutans* and *S. oralis)* after 24 h incubation at 37 °C compared to native QCD-*g*-CS (Fig. 6). The % reduction of microbial colony of QCD-*g*-CS samples, either native QCD-*g*-CSs or EG loaded with QCD-*g*-CSs, was compared to those of free EG. If the relative values were higher than 1, it indicates an enhanced reduction of microorganism. The antimicrobial activities of QCD-*g*-CS-EG inclusion complex could be overall ranked as *C. albican* > *S. mutans* > *S. oralis*. In comparison to native QCD-*g*-CS, almost all QCD-*g*-CS-EG inclusion complex demonstrated higher % reduction. The QCD11-*g*-CS-EG inclusion complex showed the highest antimicrobial activity against observed microorganism. It is likely that dominant microorganism reduction of QCD11-*g*-CS-EG would come from quaternary ammonium moieties of the derivatives as well as the highest %EE. Improved antimicrobial activity can be attributed to increased solubility of EG in the aqueous phase due to the presence of QCD-*g*-CS, hence improved interactions between EG and microorganisms. It is known that both EG and CS have antimicrobial activity (Kumar et al., 2004; Rabea, Badawy, Stevens, Smagghe, & Steurbaut, 2003) as well as our report of both QCS and QCD-*g*-CSs against *C. albican*, *S. mutans* and *S. oralis* (Gonil et al., 2011). Therefore, a presence of both EG and QCD-*g*-CSs as inclusion complex resulted in synergistic effect on antimicrobial activity. However, different extent of antimicrobial activity from QCD-*g*-CSs on each microorganism (*C. albican* > *S. mutans* > *S. oralis*) might be due to the fundamental differences in microbial cell wall between fungi and bacteria (Franklin & Snow, 1981). Similar result has been observed (Rabea et al., 2003) where spoilage yeasts or *C. albican* were more sensitive to the CS than Gram-positive and Gram-negative bacteria.

4. Conclusion

New water-soluble βCD-grafted chitosan derivatives (QCD-*g*-CS) and their inclusion complex with eugenol (EG) were investigated. Inclusion complex between QCD-g-CS and EG was confirmed by FTIR. However, self-aggregated formation of QCD-g-CS was also found in aqueous system according to fluorescence and TEM study. CAC values of QCD11*g*-CS and QCD5-*g*-CS were similar and lower than that of QCD23-*g*-CS, indicating that self-aggregated formation was more preferable for QCD11*g*-CS and QCD5-*g*-CS. EG was included both in βCD hydrophobic cavity of QCD-*g*-CS and hydrophobic core of QCD-*g*-CS self-aggregates, resulting in varying extent of EG entrapment efficiencies. The degree of N-substitution of βCD (DS) in QCD-*g*-CS plays an important role on their physical properties. The highest amount of EG can be entrapped both within βCD cavity and hydrophobic core of QCD11-*g*-CS than other QCD-*g*-CSs. This correlated well with simulation study where total free energy of QCD11-*g*-CS was the most preferable and QCD23-*g*-CS was the least. Steric hindrance of βCD itself or remained tosylate group into the QCD-*g*-CS backbone play a role on complex formation between EG and QCD-*g*-CS. High DS of QCD23-*g*-CS resulted in steric hindrance on chitosan chain, hence lower the formation of self-aggregates and EG entrapment efficiencies. Mucoadhesive responses of QCD-*g*-CS entrapped with EG were not significantly different from native QCD-*g*-CS. The greatest mucoadhesion was found from QCD11-*g*-CS, in which electrostatic interaction majorly governed the adhesion between mucin and the derivatives. The QCD11-*g*-CS-EG inclusion complex showed a good candidate in terms of high EG entrapment, mucoadhesive property and antimicrobial activity for mucosal drug delivery.

Acknowledgments

The authors wish to acknowledge the financial support from the Research, Development and Engineering (RD&E) through the National Nanotechnology Center (NANOTEC), National Science and Technology Development Agency (NSTDA), Thailand (Project No. NN-B-22-EN7-94-51-20). Technical assistance from Dr. Boonsong Sutapun, Photonics Technology Laboratory, the National Electronics and Computer Technology Center (NECTEC) are appreciated.

References

Anantachaisilp, S., Meejoo, S. S., Treetong, A., Pratontep, S., Puttipipatkhachorn, S., & Ruktanonchai, U. R. (2010). Chemical and structural investigation of lipid nanoparticles: Drug-lipid interaction and molecular distribution. *Nanotechnology*, *21*, 12512.

Auzely-Velty, R., Djedaini-Pilard, F., Desert, S., Perly, B., & Zemb, T. (2000). Micellization of hydrophobically modified cyclodextrins. Micellar structure. *Langmuir*, *16*, 3727–3734.

Bibby, D. C., Davies, N. M., & Tucker, I. G. (1999). Poly(acrylic) microspheres containing β-cyclodextri: Loading and *in vitro* release of two dyes. *International Journal of Pharmaceutics*, *187*, 243–250.

Brady, B., Lynam, N., O'Sullivan, T., Ahern, C., & Darey, R. (2000). 6A-O-p-toluenesulfonyl-β-cyclodextrin: (β-Cyclodextrin, 6A-(4-methylbenzenesulfonate)). *Organic Syntheses*, *77*, 220–224.

Challa, R., Ahuja, A., Ali, J., & Khar, R. K. (2005). Cyclodextrins in drug delivery: An updated review. *AAPS PharmSciTech*, *6*, E329–E357.

Coleman, A. W., Nicolis, I., Keller, N., & Dalbiez, J. P. (1992). Aggregation of cyclodextrins: An explanation of the abnormal solubility of %cyclodextrin. *Journal of Inclusion Phenomena and Macrocyclic Chemistry*, *13*, 139–143.

Fermeglia, M., Ferrone, M., Lodi, A., & Prici, S. (2003). Host-guest inclusion complexes between anticancer drugs and β-cyclodextrin: Computational studies. *Carbohydrate Polymer*, *53*, 15–44.

Franklin, T. J., & Snow, G. A. (1981). *Biochemistry of antimicrobial action* (3rd ed.). London: Chapman and Hall.

Gonil, P., Sajomsang, W., Rungsardthong, U. R., Pimpha, N., Sramala, I., Nuchuchua, O., et al. (2011). Novel quaternized chitosan containing β-cyclodextrin moiety: Synthesis, characterization and antimicrobial activity. *Carbohydrate Polymer*, *83*, 905–913.

He, Y., Fu, P., Shen, X., & Gao, H. (2008). Cyclodextrin-based aggregates and characterization by microscopy. *Micron*, *39*, 495–516.

Kalemba, D., & Kunicka, A. (2003). Antibacterial and antifungal properties of essential oils. *Current Medicinal Chemistry*, *10*, 813–829.

Kumar, R. M. N. V., Muzzarelli, R. A. A., Muzzarelli, C., Sashiwa, H., & Domb, A. J. (2004). Chitosan chemistry and pharmaceutical perspectives. *Chemical Reviews*, *104*, 6017–6084.

Muzzarelli, R. A. A., Tarsi, R., Filippini, O., Giovanetti, E., Biagini, G., & Varaldo, P. E. (1990). Antimicrobial properties of N-carboxybutyl chitosan. *Antimicrobial Agents and Chemotherapy*, *34*, 2019–2023.

Ohkubo, T., & Shibata, M. (1997). The selective capsaicin antagonist capsazepine abolishes the antinociceptive action of eugenol and guaiacol. *Journal of Dental Research*, *76*, 848–851.

Ou, H. C., Chou, F. P., Lin, T. M., Yang, C. H., & Sheu, W. H. H. (2006). Protective effects of eugenol against oxidized LDL-introduced cytotoxicity and adhesion molecule expression in endothelial cells. *Food and Chemical Toxicology*, *44*, 1485–1495.

Petchsangsai, M., Sajomsang, W., Gonil, P., Nuchuchua, O., Sutapun, B., Puttipipatkhachorn, S., et al. (2011). A water-soluble methylated N-(4-N,

N-dimethylaminocinnamyl) chitosan chloride as novel mucoadhesive polymeric nanocomplex platform for sustained-release drug delivery. *Carbohydrate Polymer*, *73*, 1263–1273.

Pitha, J., Harman, S. M., & Michel, M. E. (1986). Hydrophilic cyclodextrin derivatives enable effective oral administration of steroidal hormones. *International Journal of Pharmaceutics*, *75*, 165–167.

Prabaharan, M., & Gong, S. (2008). Novel thiolated carboxymethyl chitosan-g-β-cyclodextrin as mucoadhesive hydrophobic drug delivery carriers. *Carbohydrate Polymer*, *73*, 117–125.

Prabaharan, M., & Jayakumar, R. (2009). Chitosan-graft-β-cyclodextrin scaffolds with controlled drug release capability for tissue engineering applications. *International Journal of Biological Macromolecules*, *44*, 320–325.

Prabaharan, M., & Mano, J. F. (2005). Hydroxypropyl chitosan bearing β-cyclodextrin cavities: Synthesis and slow release of its inclusion complex with a model hydrophobic drug. *Macromolecular Bioscience*, *5*, 965–973.

Rabea, E. I., Badawy, M. E. T., Stevens, C. V., Smagghe, G., & Steurbaut, W. (2003). Chitosan as antimicrobial agent: Applications and mode of action. *Biomacromolecules*, *4*, 1457–1465.

Rossi, S., Ferrari, F., Bonferoni, M. C., & Caramella, C. (2001). Characterization of chitosan hydrochloride-mucin rheological interaction: Influence of polymer concentration and polymer:mucin weight ratio. *European Journal of Pharmaceutical Sciences*, *12*, 479–485.

Sajomsang, W., Gonil, P., Ruktanonchai, U. R., Pimpha, N., Sramala, I., Nuchuchua, O., et al. (2011). Self-aggregates formation and mucoadhesive property of water-soluble-cyclodextrin grafted with chitosan. *International Journal of Biological Macromolecules*, *48*, 589–595.

Shumaker-Parry, J. S., Aebersold, R., & Campbell, C. T. (2004). Parallel, quantitative measurement of protein binding to a 120-element double-stranded DNA array in real time using surface plasmon resonance microscopy. *Analytical Chemistry*, *76*, 2071–2082.

Smart, J. D. (2005). The basics and underlying mechanisms of mucoadhesion. *Advanced Drug Delivery Reviews*, *57*, 1556–1568.

Son, K. H., Kwon, S. Y., Kim, H. P., Chang, H. W., & Kang, S. S. (1998). Constituents from Syzygium aromaticum Merr. et Perry. *Natural Product Sciences*, *4*, 263–267.

Svensson, O., Thuresson, K., & Arnebrant, T. (2008). Interactions between chitosan-modified particles and mucin-coated surfaces. *Journal of Colloid and Interface Science*, *325*, 346–350.

Szejtli, J. (2004). Past, present, and future of cyclodextrin research. *Pure and Applied Chemistry*, *76*, 1825–1845.

Takeuchi, H., Thongborisute, J., Matsui, Y., Yamamoto, H., & Kawashima, Y. (2005). Novel mucoadhesion tests for polymers and polymer-coated particles to design optimal mucoadhesive drug delivery systems. *Advanced Drug Delivery Reviews*, *57*, 1583–1594.

Tan, Y., & Liu, C. G. (2009). Self-aggregated nanoparticles from linoleic acid modified carboxymethyl chitosan: Synthesis, characterization and application *in vitro*. *Colloids and Surfaces B: Biointerfaces*, *69*, 178–182.

Thongborisute, J., & Takeuchi, H. (2008). Evaluation of mucoadhesiveness of polymers by BIACORE method and mucin-particle method. *International Journal of Pharmaceutics*, *354*, 204–209.

Yang, Y., & Song, L. X. (2005). Study on the inclusion compounds of eugenol with α-, β-, γ- and heptakis (2,6-di-O-methyl)-β-cyclodextrins. *Journal of Inclusion Phenomena and Macrocyclic Chemistry*, *53*, 27–33.

Yoshida, A., Arima, H., Uekama, K., & Pitha, J. (1988). Pharmaceutical evaluation of hydroxyalkyl ethers of β-cyclodextrins. *International Journal of Pharmaceutics*, *46*, 217–222.

Zhan, H., Jiang, Z. T., Wang, Y., Li, R., & Dong, T. S. (2008). Molecular microcapsules and inclusion interactions of eugenol with β-cyclodextrin and its derivatives. *European Food Research Technology*, *227*, 1507–1513.

Zhang, J., Feng, K., Cuddihy, M., Kotov, N. A., & Ma, P. X. (2010). Spontaneous formation of temperature-responsive assemblies by molecular recognition of a β-cyclodextrin-containing block copolymer and poly(N-isopropylacrylamide). *Soft Matter*, *6*, 610–617.